

# 360 Panorama Synthesis from a Sparse Set of Images with Unknown FOV

Julius Surya Sumantri      In Kyu Park

{julius.taeng@gmail, pik@inha.ac.kr}

Dept. of Information and Communication Engineering, Inha University, Incheon 22212, Korea

## Abstract

360° images represent scenes captured in all possible viewing directions. They enable viewers to navigate freely around the scene and thus provide an immersive experience. Conversely, conventional images represent scenes in a single viewing direction. These images are captured with a small or limited field of view. As a result, only some parts of the scenes are observed, and valuable information about the surroundings is lost. We propose a learning-based approach that reconstructs the scene in  $360^\circ \times 180^\circ$  from conventional images. This approach first estimates the field of view of input images relative to the panorama. The estimated field of view is then used as the prior for synthesizing a high-resolution 360° panoramic output. Experimental results demonstrate that our approach outperforms alternative method and is robust enough to synthesize real-world data (e.g. scenes captured using smartphones).

## 1. Introduction

Images are limited to the boundaries of what camera devices can capture. An image with a narrow field of view sees only a small part of a given scene. After the scene is captured, the viewer obtains no information on what lies beyond the image. 360° panoramic images overcome this limitation through a wide field of view. As a result, all information on scenes across the horizontal and vertical viewing directions is captured. This imagery provides viewers with an outward-looking view of scenes and the freedom to shift their viewing directions accordingly.

360° panoramic images are widely used in many fields, such as virtual environments, display system, free-viewpoint videos, and environment modeling. Although capturing scenes using 360° is easy, not everyone has these particular devices. Meanwhile, most people own and carry smartphones that are equipped with decent cameras.

Smartphones application such as Google Camera allow users to capture 360° panoramic scenes. However, the process requires careful interaction from users. A target scene must be mapped to a virtual grid while covering all possi-

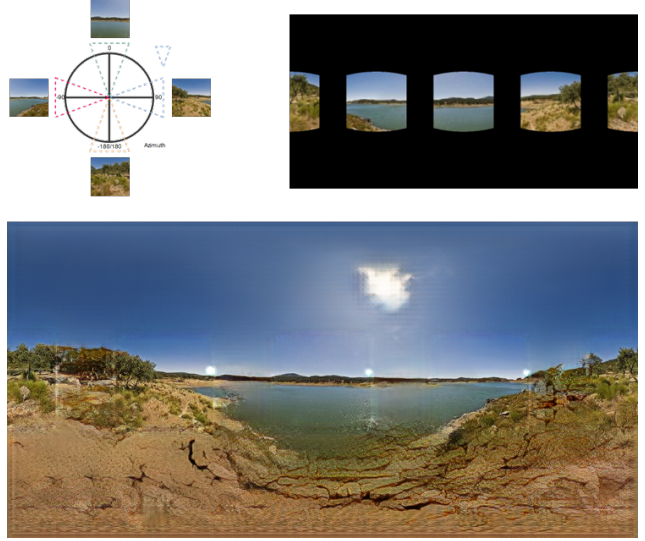


Figure 1: Overview of the proposed work. Our work synthesizes 360° panorama from partial input. The inputs are captured in four different horizontal viewing directions. They are captured in sequence with small field of view and no overlapping.

ble viewing directions. This requirement makes the process inconvenient and time-consuming. Another alternative is to take images from smartphones in "panoramic mode". Users must capture scenes in a contiguous manner, and can only cover the horizontal viewing direction.

We aim to solve the problem of synthesizing full 360° panoramic images from a sequence of images captured with a wide baseline. These sequences are partial observations of scenes captured from four viewing directions as shown in Figure 1. In particular, the center view is in the middle of a compass rose looking outward to the north, west, east, and south. The input sequences have a small and unknown field of view, resulting in regions with missing pixels in panoramic representation.

This problem is an ill-posed and highly challenging task in the computational domain. Nonetheless, by learning the statistics of many general scenes to interpret their true dis-

tribution, we can train our model to significantly extrapolate and interpolate scenes to form full panoramic images.

To the best of our knowledge, the current work is the first to address the synthesis of 360° panoramic images from conventional images. The contribution of this paper can be summarized as follows.

- We propose a model to estimate the relative field of view from input sequences with an unknown field of view and no overlap to help panorama synthesis process.
- To provide a meaningful scene representation, We design a network to synthesize panoramic images with a continuous high-resolution output up to  $1024 \times 512$ .
- We represent the panoramic output in which all surrounding information is captured continuously without severe stitching artifacts or pixel inconsistency.

## 2. Related Work

Generating a scene with a large field of view from multiple observations is a long-term task for multi-view algorithms [5, 22]. Panoramic images can be generated from several overlapping inputs by stitching them together. This algorithm relies on highly overlapping regions of inputs and feature matching. In contrast to these works, our inputs do not have any overlapping between them.

**Image Inpainting and Completion** Inpainting methods interpolate missing or occluded regions of an input by filling these regions with plausible pixels. Most algorithms rely on neighboring pixels to propagate the pixel information to target regions [2, 4]. These methods generally handle images with narrow holes and do not perform well on large holes [3, 15]. Liu *et al.* [17] recently proposed to solve arbitrary holes by training convolutional neural networks (CNN). To solve an inpainting task, they use partial convolution with binary a mask as prior for the missing holes. Iizuka *et al.* [10] propose local and global discriminator networks to maintain consistent results for missing regions. However, these methods applied to known boundary images and are not suitable for handling images beyond the field of view.

**Novel View Synthesis** This method generates images with different viewing directions. The task includes generating different poses transformed by a limited rotation [23]. Dosovitskiy [6] proposed a learning based approach to synthesize diverse view variations; this method is capable of rendering different models of inputs. Zhou *et al.* [30] proposed appearance flow method to synthesize object with extreme view variations, but this method is limited to a single object with a homogeneous background. These existing

studies handled objects with limited shape variances and inward looking view, while our work handles outward looking views with relatively diverse scenes.

**Beyond Camera Viewpoint** Framebreak [29] yields impressive results in generating partial panorama from images with a small field of view. The method requires the manual selection of reference images to be aligned with input images. Guided patch-based texture synthesis is then used to generate missing pixels. The process requires reference images with high similarity with the input.

Xiao *et al.* [27] predicted the viewpoint of a given panoramic observation. The prediction generates rough panorama structure and compass-like prediction in determining the location of the viewpoint in 360°. Georgoulis *et al.* [7] estimated environmental map from the reflectance properties of input images. They utilized these properties from a foreground object to estimate the background environment in a panoramic representation. In contrast to these works, ours does not rely on reference images as the input, and it synthesizes actual panoramic imagery.

**Deep Neural Network (DNN)** In recent years, learning-based methods rooted in DNN have achieved remarkable success and are widely used to solve various tasks on computational domain. The DNN encodes millions of parameters that are suitable for handling tasks that require complex data modeling. Generative models such as generative adversarial networks (GAN) [8] also enjoy tremendous success in generating novel pixels by learning prior distribution from true data.

The generative adversarial network works well on images with low resolutions (*e.g.*  $128 \times 128$ ) and can even compete with human performance, but it mainly struggles on images with high-resolution and suffers from instability problem during training. During the last few years, several architectures [1, 18, 19] have been proposed to overcome these limitations and solve various tasks.

Image-to-image translation proposed by Isola *et al.* [12] translates input domain to another domain using input and output for training. This work was extended by Wang *et al.* [25] to synthesize high-resolution images from input semantic labels. Despite the results, their work relied on semantic labels which are not always available and practical for most inputs. Karras *et al.* [13] obtained impressive results in generating images with high-resolution using GAN, trained in an unconditional manner. The network can synthesize facial images with great details but it requires a large amount of computing power.

We take inspiration to solve the synthesis task using the GAN framework. Unlike previous works, ours adopt a network that is tailored to output images with diverse scenes, high-resolution and inexpensive computing power.

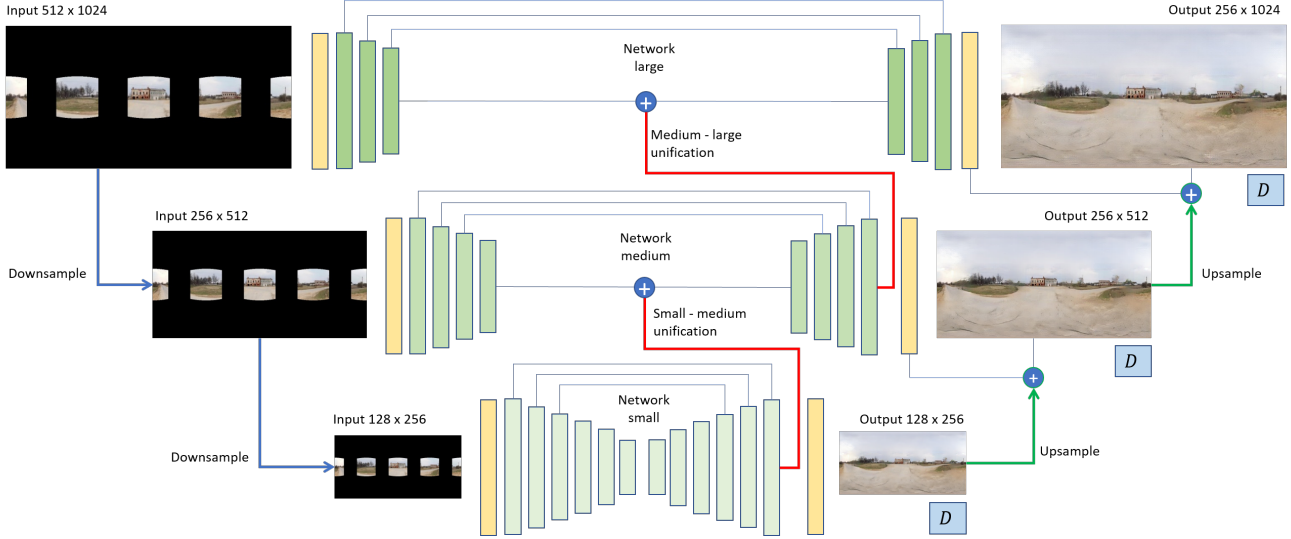


Figure 2: The architecture of the proposed network. The network takes three input images at different scale level: small, medium, and large. At each scale, each (sub)network learns to synthesize images with the same scale as the input with supervision from the discriminator network  $D$ . The scale and network capacity are increased gradually on each level. Network at the previous scale is connected and unified via residual connection. Small scale network only yields single output, which is trained directly to minimize the pixel loss. At the larger scale, previous output from smaller scale is no longer trained to minimize the pixel loss. Instead, the output is treated as the residual by upsampling and adding it to the current scale.

### 3. Overview and Background

#### 3.1. Overview

We design and utilize a CNN with GAN-based framework, as visualized in Figure 2, to address the synthesis problem. The proposed approach consists of two processing stages. The first stage is the field of view estimation network, in which the main task is to predict input images' field of view relative to  $360^\circ$  panoramic images. The second stage is the synthesis network fed with processed inputs from the first stage mainly to estimate the missing pixels in the panorama.

The inputs to our network are four ordered sequences of images. They have an unknown small field of view, that is separated by a large baseline. Each observation is performed on four direction of the compass rose: north, west, south, and east respectively as shown in Figure 3. If the scene is captured from each direction with a  $90^\circ$  field of view and 1:1 aspect ratio, a horizontal panorama can be formed by concatenating them together.

By folding these images into a planar plane, we have a panorama represented in the form of the cube map. The cube map forms a pattern with missing regions, but it has similar properties to 2D images. Meanwhile, the equirectangular format can be formed by warping the cube map into a sphere. This format results in a distorted input, but it preserves the continuity between vertical and horizontal axes

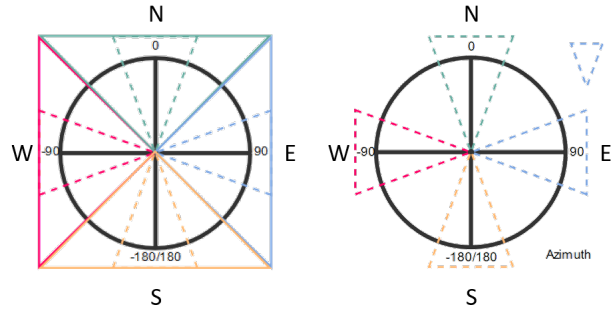


Figure 3: Field of view visualization. The triangles are observation field of view looking from the vertical center viewpoint. Solid triangles are observation with  $90^\circ$  field of view. This results in  $360^\circ$  panorama from four horizontal view point: north, west, south, and east. Dashed triangles are observations with less than  $90^\circ$  field of view which form partial panorama.

(no missing regions). For these reasons, the field of view estimation network takes the input and produces the output in a cube map format, while the panorama synthesis takes the input and output in the equirectangular format

#### 3.2. Conditional GAN

Conditional GAN consists of a generator network  $G$  and discriminator network  $D$  conditioned with an input label.

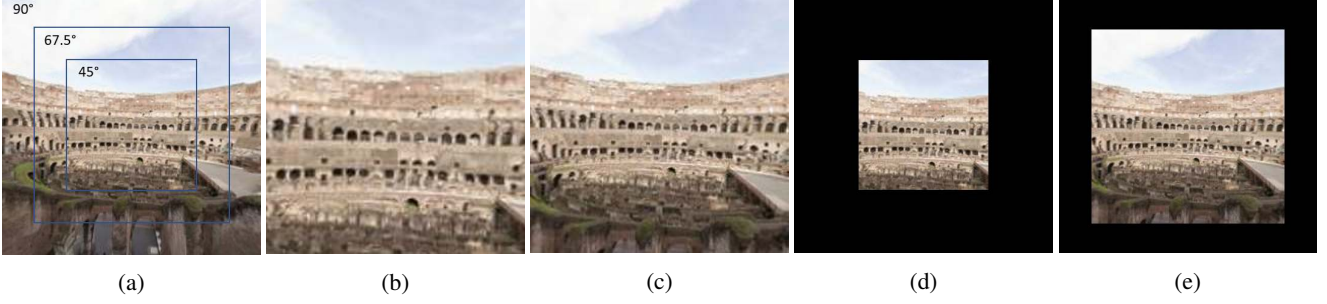


Figure 4: Relative field of view. (a) shows image with  $90^\circ$  field of view. The blue line shows scene coverage of different field of view. (b) and (c) shows images at captured in  $45^\circ$  and  $67.5^\circ$  field of view. The outputs of our field estimation network are shown in (d) and (e). The black region is the empty pixel, and image in the center is rescaled to match the panorama field of view.

Pixel loss is employed to supervised loss to facilitate the synthesis task. In practice  $L1$  or  $L2$  loss can be minimized, however,  $L1$  loss is more preferable as it produces sharper results. The network objective function is defined as

$$L_{adv}(G, D) = \mathbf{E}_{I_p} [\log D(I_i, I_p)] + \mathbf{E}_{I_i, \hat{I}_p} [\log(1 - D(I_i, \hat{I}_p))], \quad (1)$$

$$L_{pix} = \mathbf{E}_{I_p, \hat{I}_p} [||I_p - \hat{I}_p||_1], \quad (2)$$

where  $I_i$  is the input image and  $\hat{I}_p$  is the output from generator  $G(I_i)$ . The pixel loss is defined as the  $L1$  distance between the ground-truth panorama  $I_p$  and  $\hat{I}_p$ . The overall loss for the network is defined as

$$L = \arg \min_G \max_D L_{adv} + \lambda L_{pix}, \quad (3)$$

which is the total adversarial GAN loss, with the pixel loss scaled by  $\lambda$  constant factor.

## 4. Proposed Approach

### 4.1. Field of View Estimation

We define the scenes in four directions of compass rose as  $I = [I_n, I_w, I_s, I_e]$  for the north, west, east and south direction respectively. The typical scenes have a field of view less than  $90^\circ$ . As a result, they do not form any connection or overlapping when concatenated.  $I$  forms disconnected partial panorama on the horizontal axis and is used as the network input. For this work, we do not account for the input on the vertical axis.

The CNN architecture is utilized to solve the estimation task. Images with a smaller field of view only presents a smaller portion of the scenes as illustrated in Figure 4. To relax the task, we first assume that images with full  $90^\circ$  field of view have same size with other smaller field of view images. Therefore by rescaling these images, estimated field

of view which corresponds to each viewing directions can be obtained. Note that this approach does not estimate the actual field of view like other similar work [26]. The main goal of this network is not to estimate the most accurate field of view, but instead served as a constraint to help the synthesis process.

The output from the network is  $N$  number of vectors representing the field of view. Input from the network is rescaled and padded with empty pixels to fill the missing region. The size of missing region depends on the estimated field of view, a larger field of view means less empty pixels as visualized in Figure 4. In particular, images with  $90^\circ$  field of view on each viewing direction form the full panorama with no empty pixels.

The field of view estimation task is treated as a multi-class classification task. Softmax cross entropy loss is used as the objective functions, defined as follows.

$$H = - \sum_i^N \{ \tilde{y}_i \log(y_i) + (1 - \tilde{y}_i) \log(1 - y_i) \}, \quad (4)$$

where  $\tilde{y}$  is the predicted output and  $y$  is the ground-truth label.

### 4.2. Panorama Synthesis

Generating high-resolution images using GAN is a challenging task due to stability problems during the training process. We propose a conditional GAN-based framework that can synthesize images with a high-resolution output. To make the task possible, we treat the problem with a hierarchical approach. Similar to an image pyramid, the task is decomposed into synthesizing images with different scales. Images with high-resolutions have more information distribution in space relative to lower resolution images. In this case, training progress is difficult to realize. Instead of aiming for the global minima in a single run, in which the network might run into an problem during training, we enforce



the network to learn step by step how to achieve the local minima on each hierarchy. This step can be regarded as providing soft guidance to help the network converge.

For this work, we decompose the input images into three hierarchies, namely, small, medium, and large scale. The large scale is the original panorama with  $512 \times 1024$  resolution. The medium scale is reduced by the scale factor of 2 from the original scale with  $256 \times 512$  resolution. The small scale is reduced by the scale factor of 4 with  $128 \times 256$  resolution. The training process is performed separately on each scale.

The input to the network includes processed images from the field of view estimation network; it is defined as  $I_i = [\hat{I}_n, \hat{I}_w, \hat{I}_s, \hat{I}_e]$ . This input represents the missing regions with empty pixels in the cube map panorama. Essentially feeding the cube map input to the network is possible, but the DNN architecture is mainly built upon convolutional operations. These operators do not account for pixel continuity in horizontal and vertical directions. As a result, when each of output of the cube map region is stitched, the resulting panorama presents severe artifacts. Therefore, we warp the processed images to form an equirectangular panoramic representation. This format also reduces the resolution of the images and minimizes the memory footprint.

#### 4.2.1 Unified Generator

The generator consists of three networks, namely,  $G^s, G^m, G^l$ , each of which corresponds to different scales. We utilize the smallest scale generator as the base generator for the entire training process. The base generator is built with a skip connection [21] to maintain the relation of low level and high level features. The training process starts from images with  $128 \times 256$  resolution as the smallest resolution. To train the next hierarchy, we unify the base generator  $G^s$  with generator  $G^m$ . In the largest scale, generator  $G^l$  is unified with  $G^m$  and  $G^s$  to form a single generator with increased capacity. The weight parameters trained from the small-scale network are reused in the large-scale one. During the training process in the medium-scale network, the trained weight is reused and fine-tuned to produce medium resolution images. The training process for the next scale follows the same rule until the original scale is reached.

Generator unification is employed with residual connection [9]. The residual connection serves as the connector for different hierarchies and prevents overfitting as the network deepens. In the case of multiple inputs–outputs, each generator has extra layers for bridging the inputs and outputs. The input bridge layers are used to map the lower dimensional RGB images to the network’s higher dimensional channel. At the same time, the output bridge layers are used to map the higher dimensional channel to the RGB channel. These layers are employed to preserve the con-

sistency of the network structure and thereby ensure proper entry and exit points in the network. The result should make unification possible. The latest layer is connected to a high hierarchy and the output bridge.

At the smallest scale, the network directly learns the pixel relationship between the predicted output and the ground-truth images. We add the residual properties at the medium- and large-scale networks. During the training of the medium-scale network, we keep the input and output bridges from the small-scale network.

#### 4.2.2 Multiscale Residual

The base generator takes the input from small-scale images and outputs small-scale panorama. This small-scale output is then used as the residual by performing upsampling operations and then added to the medium-scale panorama output. The same rule follows for training the large-scale images by keeping the input bridge of the small- and medium-scale images, followed by the residual from the output bridge. The function is defined as

$$\hat{I}_p^l = G^l(I_i^l) + f(\hat{I}_p^m), \quad (5)$$

$$\hat{I}_p^m = G^m(I_i^m) + f(\hat{I}_p^s), \quad (6)$$

$$\hat{I}_p^s = G^s(I_i^s), \quad (7)$$

where  $\hat{I}_p^*$  is the panorama output and  $I_i^*$  is the input on each scale.  $G$  denotes the network function and  $f$  denotes the upsampling operations.

#### 4.2.3 Multi-Discriminator

Multiple discriminators on each scale, namely,  $D^s, D^m, D^l$ , are used in this work. These discriminators have the same architectures across all scales. The input for each discriminator comprises concatenated output and input images. For images with lower resolution, the input images are downsampled from the original resolution to match the output resolution. We predict  $N \times N$  patch of images instead of single logits. To further improve stability for training, we employ normalization operations. Normalization in GAN helps the network eliminate covariance shift. Batch normalization [11] is a common normalization method, but it suffers from stability problems when the batch size is small. We use a batch size of 1 across all scales to reduce the computation requirements. Therefore, the batch normalization method is not suitable for this task; we use the instance normalization [24] instead.

#### 4.3. Implementation Details

The field of view estimation network is build on convolutional blocks followed with leaky ReLU [28] activation.

The network is trained with ADAM [14] optimizer, jointly with the panorama synthesis network on the smallest scale only. We minimize the multi class cross entropy loss function, where each  $N$  vectors correspond to the predicted field of view.

Panorama synthesis network is trained on each hierarchy with the corresponding generator and discriminator. The generator is built on a residual connection to unify the network structure and skip connection on each generator layers. The networks use convolutional blocks followed with instance normalization and leaky ReLU activation except on the input bridge and output bridge. The input bridge maps the three RGB channels into 64 dimensional layers and the output bridge maps 64 dimensional channels back to RGB channels. We use ADAM optimizer with learning rate  $\alpha = 0.0002$ ,  $\beta_1 = 0.5$ , and  $\beta_2 = 0.99$ .

## 5. Experimental Result

### 5.1. Dataset

For the training and evaluation of the proposed network, we use outdoor panoramic images from the SUN360 [27] dataset. We split the dataset into the training set (80%) and the testing set (20%). The dataset contains around 40,000 images with different scene variations rendered in equirectangular format. To accommodate the data with our framework, we render the panorama to a cube map format by warping it to the planar plane. We split the viewing direction into the four horizontal sides of the cube. The vertical center is located at  $0^\circ$ , and the horizontal center is located at  $0^\circ$ ,  $90^\circ$ ,  $180^\circ$ , and  $270^\circ$ . The field of view for each horizontal view is the same, that is, it is generated randomly from  $45^\circ$  to  $75^\circ$ . The images are normalized to  $[-1, 1]$  for stability during training.

### 5.2. Qualitative Evaluation

High resolution synthesis using conditional GAN is not widely studied. pix2pixHD [25] is mainly presented to synthesize images from semantic labels. However, the conditional properties of GAN in the framework can be used as an alternative approach in our case. The results are evaluated on the SUN360 test set. Our results from the test set are shown in Figure 6. We successfully synthesize  $360^\circ$  panorama from partial observations. Although the baseline work performs well on semantic to image prediction, and facial synthesis. It is shown that our results clearly outperform pix2pixHD [25].

We believe that this difference is due to the relatively challenging task we are solving and due to the fact that the missing regions in most problems are larger than visible regions. The outdoor scene dataset also exhibits greater variance than does the dataset of faces or road scenes in semantic-to-image synthesis. The typical results from the



Figure 5: Cube map warping. The output trained on cube map format has problem in equirectangular warping. The warping produces panorama with discontinuity effect across the vertical and horizontal axis.

baseline work are synthesized smoothly, but they appear cartoonish, whereas our results are relatively sharp. For the challenging scenes shown in Figure 8, where most of the scenes are covered with trees and foliage, both methods fail to synthesize plausible results. The synthesized results are severely disrupted due to scene complexity.

Accurate semantic label maps can help the network understand a given object in a scene. In this case, the synthesis results may be improved. However, datasets for  $360^\circ$  panorama scene prediction, understanding, manipulation, and synthesis remain limited. Dataset creation may be worth exploring in future works.

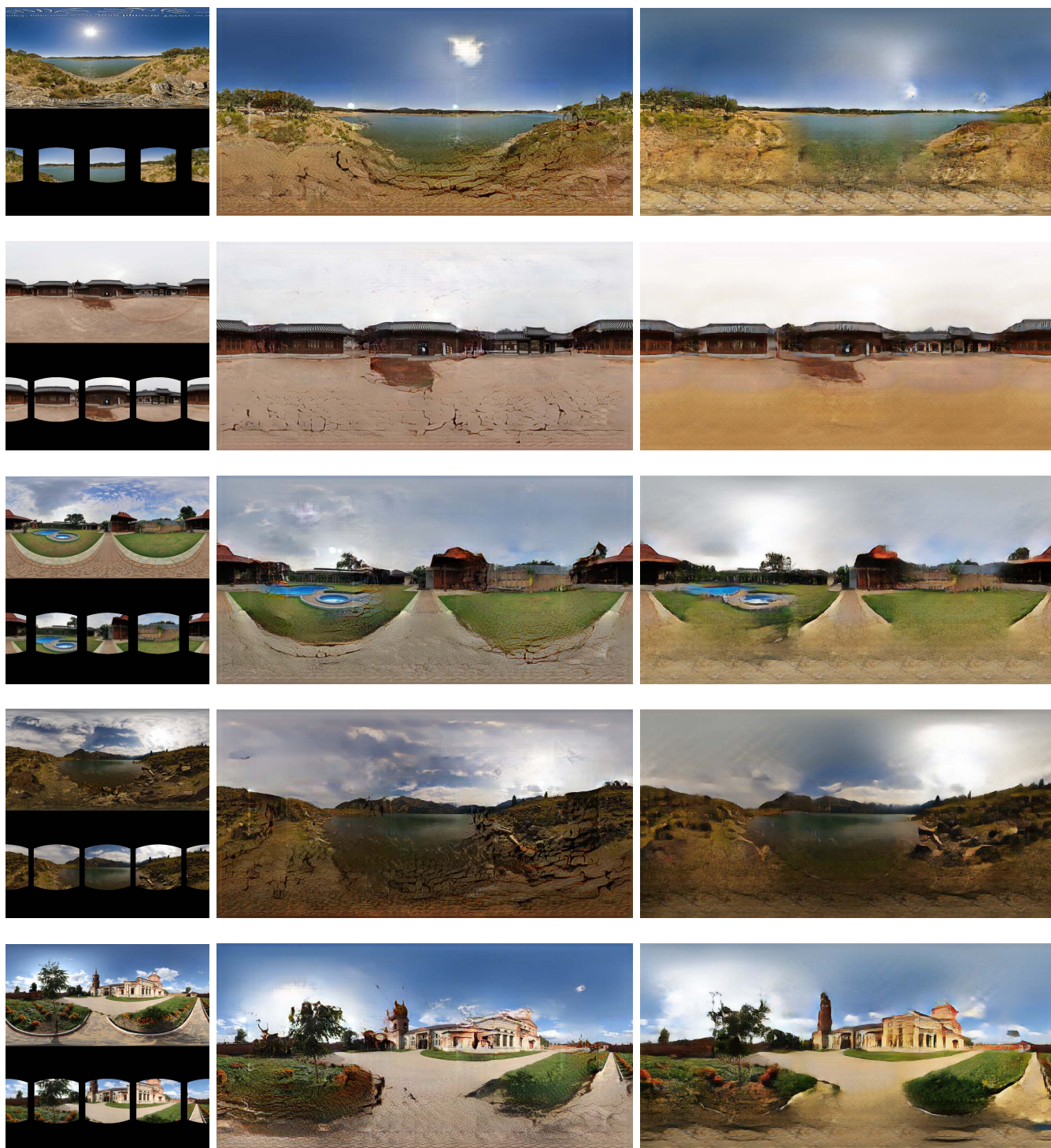
Although we successfully synthesize the panorama in high-resolution, it is far from being perfect. The field of view estimation network does not estimate the actual field of view, and this restriction serves as a constraint for the network. Developing an algorithm capable of predicting the actual field of view panorama and synthesizing all surrounding scenes would be beneficial. The work is currently limited to handling inputs in ordered and known locations. The development of an algorithm for estimating the sequences and orders of scenes without overlapping is an interesting problem to tackle.

### 5.3. Real-World Data in the Wild

Furthermore, we show additional results for real-world scenes taken with smartphones, as shown in Figure 7. Our capturing process is more convenient than that of other approaches as it only requires a few seconds to capture four scenes in different view directions instead of capturing scenes continuously. The scenes can be captured with a rough estimation of four compass view directions, and plausible results can still be generated.

We show our result that is trained on the cube-map format to synthesize the images over all missing regions to preserve the continuity. However, panorama images are truly meaningful images when it is visualized in the free view point rendering by warping it to equirectangular format. It is shown in Figure 5 the output after the warping produce discontinuity in the cube-map boundary and different color.





Ground-truth and input

Proposed

pix2pixHD [25]

Figure 6: Synthesized results. We visualize our synthesized 360° panoramas trained on  $512 \times 1024$  resolution. The results are compared with conditional GAN framework pix2pixHD [25]. Our proposed work produces sharper panorama images where the baseline work produces smoother and blurrier results.



Figure 7: Real-world data results. We synthesize  $512 \times 1024$  panorama output from real-world data captured with smartphone. The scenes are captured in four viewing direction with unknown field of view.



Figure 8: Failure cases. Our network face difficulty in synthesizing good results on (a) building shape and (b) scene with numerous trees and foliage. Scenes with trees and foliage have more complex structures and distribution than buildings, which severely disrupt the overall output.

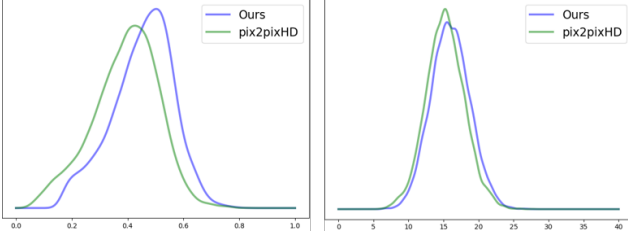


Figure 9: Quantitative result. Histogram distribution on SSIM and PSNR. The proposed work outperforms the previous work quantitatively.

#### 5.4. Quantitative Evaluation

Generative models evaluation metrics are not well established. Each metrics has advantages and disadvantages. Several works on super resolution [16] and image synthesis [20] using the generative model employ structural-similarity (SSIM) and peak signal to noise ratio (PSNR). We evaluate the dense histogram distribution of SSIM and PSNR as shown in Figure 9 to measure the network overall performance. The proposed work yields better SSIM distribution over the baseline work, while PSNR distribution has

Metric	Ours	pix2pixHD [25]
SSIM	0.4528	0.3921
PSNR	15.9711	15.2634

Table 1: SSIM and PSNR (in dB) score between the proposed work and the baseline work

a slight improvement. Average SSIM and PSNR are shown in Table 1.

## 6. Conclusion

In this work, we present the synthesis of  $360^\circ \times 180^\circ$  panorama from sequences of wide baseline partial images. Our work generated  $512 \times 1024$  high resolution panoramic images by estimating the field of view, and synthesizing them in hierarchical manner. The experimental results show that the proposed work outperforms the baseline work quantitatively and qualitatively. The proposed work can be generalized to generate real-world scenes captured with smartphones camera. We believe that our can be applied to different tasks to produce high-resolution output and hope that this work would pioneer efforts to achieve improvement.



## References

- [1] M. Arjovsky, S. Chintala, and L. Bottou. Wasserstein generative adversarial networks. In *Proc. of International Conference on Machine Learning*, pages 214–223, 2017. [2](#)
- [2] C. Ballester, M. Bertalmio, V. Caselles, G. Sapiro, and J. Verdera. Filling-in by joint interpolation of vector fields and gray levels. *IEEE Transactions on image processing*, 10(8):1200–1211, August 2001. [2](#)
- [3] C. Barnes, E. Shechtman, A. Finkelstein, and D. B. Goldman. Patchmatch: A randomized correspondence algorithm for structural image editing. *ACM Transactions on Graphics*, 28(3):24:1–24:11, 2009. [2](#)
- [4] M. Bertalmio, G. Sapiro, V. Caselles, and C. Ballester. Image inpainting. In *Proc. of Computer graphics and interactive techniques*, pages 417–424, 2000. [2](#)
- [5] M. Brown and D. G. Lowe. Automatic panoramic image stitching using invariant features. *International Journal of Computer Vision*, 74(1):59–73, August 2007. [2](#)
- [6] A. Dosovitskiy, J. Tobias Springenberg, and T. Brox. Learning to generate chairs with convolutional neural networks. In *Proc. of IEEE Conference on Computer Vision and Pattern Recognition*, June 2015. [2](#)
- [7] S. Georgoulis, K. Rematas, T. Ritschel, M. Fritz, T. Tuytelaars, and L. V. Gool. What is around the camera? In *Proc. of IEEE International Conference on Computer Vision*, pages 5180–5188, October 2017. [2](#)
- [8] I. Goodfellow, J. Pouget-Abadie, M. Mirza, B. Xu, D. Warde-Farley, S. Ozair, A. Courville, and Y. Bengio. Generative adversarial nets. In *Advances in Neural Information Processing Systems*, pages 2672–2680, 2014. [2](#)
- [9] K. He, X. Zhang, S. Ren, and J. Sun. Deep residual learning for image recognition. In *Proc. of IEEE Conference on Computer Vision and Pattern Recognition*, June 2016. [5](#)
- [10] S. Iizuka, E. Simo-Serra, and H. Ishikawa. Globally and Locally Consistent Image Completion. In *ACM Transactions on Graphics*, volume 36, pages 107:1–107:14, 2017. [2](#)
- [11] S. Ioffe and C. Szegedy. Batch normalization: Accelerating deep network training by reducing internal covariate shift. In *Proc. of International Conference on Machine Learning*, pages 448–456, 2015. [5](#)
- [12] P. Isola, J.-Y. Zhu, T. Zhou, and A. A. Efros. Image-to-image translation with conditional adversarial networks. In *Proc. of IEEE Conference on Computer Vision and Pattern Recognition*, July 2017. [2](#)
- [13] T. Karras, T. Aila, S. Laine, and J. Lehtinen. Progressive growing of GANs for improved quality, stability, and variation. In *International Conference on Learning Representations*, 2018. [2](#)
- [14] D. P. Kingma and J. Ba. Adam: A method for stochastic optimization. *CoRR*, abs/1412.6980, 2014. [6](#)
- [15] V. Kwatra, I. Essa, A. Bobick, and N. Kwatra. Texture optimization for example-based synthesis. In *ACM Transactions on Graphics*, 2005. [2](#)
- [16] C. Ledig, L. Theis, F. Huszar, J. Caballero, A. Cunningham, A. Acosta, A. Aitken, A. Tejani, J. Totz, Z. Wang, and W. Shi. Photo-realistic single image super-resolution using a generative adversarial network. In *Proc. of IEEE Conference on Computer Vision and Pattern Recognition*, July 2017. [8](#)
- [17] G. Liu, F. A. Reda, K. J. Shih, T.-C. Wang, A. Tao, and B. Catanzaro. Image inpainting for irregular holes using partial convolutions. In *Proc. of European Conference on Computer Vision*, September 2018. [2](#)
- [18] M. Lucic, K. Kurach, M. Michalski, S. Gelly, and O. Bousquet. Are GANs created equal? a Large-Scale Study. *CoRR*, abs/1711.10337, 2017. [2](#)
- [19] X. Mao, Q. Li, H. Xie, R. Y. K. Lau, Z. Wang, and S. P. Smolley. Least squares generative adversarial networks. In *Proc. of IEEE International Conference on Computer Vision*, pages 2813–2821, 2017. [2](#)
- [20] K. Regmi and A. Borji. Cross-view image synthesis using conditional GANs. In *Proc. of IEEE Conference on Computer Vision and Pattern Recognition*, June 2018. [8](#)
- [21] O. Ronneberger, P. Fischer, and T. Brox. U-net: Convolutional networks for biomedical image segmentation. In *Medical Image Computing and Computer-Assisted Intervention*, volume 9351, pages 234–241, 2015. [5](#)
- [22] R. Szeliski. Image alignment and stitching: A tutorial. *Foundations and Trends in Computer Graphics and Vision*, 2(1):1–104, January 2006. [2](#)
- [23] M. Tatarchenko, A. Dosovitskiy, and T. Brox. Single-view to multi-view: Reconstructing unseen views with a convolutional network. In *Proc. of IEEE European Conference on Computer Vision*, september 2015. [2](#)
- [24] D. Ulyanov, A. Vedaldi, and V. S. Lempitsky. Instance normalization: The missing ingredient for fast stylization. *CoRR*, abs/1607.08022, 2016. [5](#)
- [25] T.-C. Wang, M.-Y. Liu, J.-Y. Zhu, A. Tao, J. Kautz, and B. Catanzaro. High-resolution image synthesis and semantic manipulation with conditional gans. In *Proceedings of the IEEE Conference on Computer Vision and Pattern Recognition*, June 2018. [2](#), [6](#), [7](#), [8](#)
- [26] S. Workman, C. Greenwell, M. Zhai, R. Baltenberger, and N. Jacobs. Deepfocal: A method for direct focal length estimation. In *IEEE International Conference on Image Processing (ICIP)*, pages 1369–1373, September 2015. [4](#)
- [27] J. Xiao, K. A. Ehinger, A. Oliva, and A. Torralba. Recognizing scene viewpoint using panoramic place representation. In *Proc. of IEEE Conference on Computer Vision and Pattern Recognition*, pages 2695–2702, June 2012. [2](#), [6](#)
- [28] B. Xu, N. Wang, T. Chen, and M. Li. Empirical evaluation of rectified activations in convolutional network. *CoRR*, abs/1505.00853, 2015. [5](#)
- [29] Y. Zhang, J. Xiao, J. Hays, and P. Tan. Framebreak: Dramatic image extrapolation by guided shift-maps. In *Proc. of IEEE Conference on Computer Vision and Pattern Recognition*, June 2013. [2](#)
- [30] T. Zhou, S. Tulsiani, W. Sun, J. Malik, and A. A. Efros. View synthesis by appearance flow. In *Proc. of IEEE European Conference on Computer Vision*, October 2016. [2](#)